PNAS RESEARCH ARTICLE | APPLIED PHYSICAL SCIENCES

Laser-emitting aqueous bioreactors for ultrasensitive bioactivity analysis

Guocheng Fang[a,b,1], Po-Hao Tseng[b,1], Jie Liao[c], Song Zhu[b], Tian Zhou[b], Hangrui Liu[d], Hui Zhu[b], Dayong Jin[e], Lan Yang[c], and Yu-Cheng Chen[b,2]

Affiliations are included on p. 8.

Edited by David McGloin, University of Technology Sydney, Sydney, NSW, Australia; received December 10, 2024; accepted July 18, 2025 by Editorial Board Member Yale E. Goldman

Water droplets, acting as natural bioreactors and optical whispering-gallery-mode (WGM) resonators, hold the potential for laser-assisted analysis. However, water/aqueous droplet lasers can only survive in air with a limited lifespan (<100 s) due to rapid evaporation, restricting their applications in bioreactions. To address this challenge, we introduce laser-emitting aqueous bioreactors (LEABs) in fluorocarbon oils. These LEABs enable stable laser emission and extend a droplet lifespan over 1,000-fold. LEABs enable the encapsulation of bioactive materials for long-term analysis with unique lasing characteristic fingerprints. The reactions within LEAB can interact with the most resonating light, enhancing detection sensitivity by over 100-fold compared to conventional WGM sensors. By integrating LEABs with microfluidic droplet technology, we demonstrated their application in monitoring enzyme activity and cellular metabolism at single-cell and multicellular levels. Furthermore, we showed the laser threshold-gated screening of single yeast. This platform can bridge the gap between laser technology and biochemical applications, broadening the scope of laser-based analysis.

microlaser | whispering-gallery-mode | aqueous droplet | optical resonator | bioreaction

Significance

Laser emission enables strong light–matter interactions, providing distinctive signals for analyzing biochemical reactions. Water droplets, as natural optical resonators, show great potential for whispering-gallery-mode (WGM) lasers. Owing to the low refractive index (RI) of water, conventional water droplet WGM lasers are restricted to air environments, suffering from rapid evaporation. To address this issue, immersing water droplets in oil is a viable strategy; however, it typically requires dense glycerol in droplets for an elevated RI. This hinders the suitability for long-term bioreaction monitoring. We developed water/aqueous droplet microlasers that can operate stably in fluorocarbon oils without additional RI-boosting additives, enabling long-term, high-throughput analysis of bioreactions through laser signals. Our platform paves the way to leverage microlasers in advanced bioactivity analysis.

Microfluidic droplet technology is a powerful tool for bioreaction analysis (1–4) that enables the encapsulation of biomolecules, bacteria, and cells within individual droplets for high-throughput analysis, typically using fluorescence as indicator signals. Most processes rely on monitoring changes in fluorescence intensity triggered by bioreactions. Consequently, it is intrinsically dependent on the weak interactions between fluorescent probes and biomolecules, which can be interfered with by background noise.

Laser harnesses stimulated emission in an optical resonator to boost interactions between fluorescent probes and biomolecules, offering high sensitivity to subtle changes, which results in unique behaviors of laser spectrum, threshold, and other characteristic optical fingerprints (5–11). These advances have driven significant progress in microscale lasers for biological applications, including single-molecule analysis, cell tracking, cellular mechanical measurement, and disease diagnosis (12–20).

Water droplets, naturally acting as optical whispering-gallery-mode (WGM) resonators, possess the potential to integrate laser emission into droplets for bioreaction analysis (21–23). However, the low refractive index (RI) of water has historically limited aqueous droplet lasers to operation in air since their debut in the early 1970s (24–30). This limitation presents two major challenges for bioapplications. First, the microdroplet lifetime is typically less than 100 s owing to rapid evaporation (31), significantly restricting their broader applications, such as long-term monitoring, which is a critical requirement for biochemical analysis. Second, manipulating water droplets in air is inherently difficult, posing significant obstacles to high-throughput analysis. To address this issue, Melikhan et al. immersed the water droplets in oil and observed the WGM laser emission when the droplets were mixed with 70% glycerol by weight (32). Although this was groundbreaking, the high glycerol concentration required limits the applications in bioanalysis.

In this study, we present laser-emitting aqueous bioreactors (LEABs) encased in fluorocarbon oil fluids (e.g., FC-84, FC-40, HFE-7500, etc.), commonly used as oil phase in microfluidics (1) (Fig. 1*A*). These bioreactors, containing organic dyes as the gain medium, generate laser emissions when excited with sufficient pump intensity. The RI of fluorocarbon oil, typically less than 1.29 (e.g., FC-84 ~1.26), enables efficient light resonance within the aqueous droplet bioreactors (RI ≥ 1.33), resulting in the LEAB lasing threshold of ~16.5 μJ mm^{-2}. Encasing LEABs in oil prevents evaporation, extending the droplet lifespan to several days.

Building on advances in droplets, LEABs can encapsulate a diverse range of bioactive materials, including biomolecules, hydrogels, bacteria, single cells, and even organoids

The authors declare no competing interest.

This article is a PNAS Direct Submission. D.M. is a guest editor invited by the Editorial Board.

[1]G.F. and P.-H.T. contributed equally to this work.

[2]To whom correspondence may be addressed. Email: yucchen@ntu.edu.sg.

This article contains supporting information online at https://www.pnas.org/lookup/suppl/doi:10.1073/pnas.2425829122/-/DCSupplemental.

Published August 22, 2025.

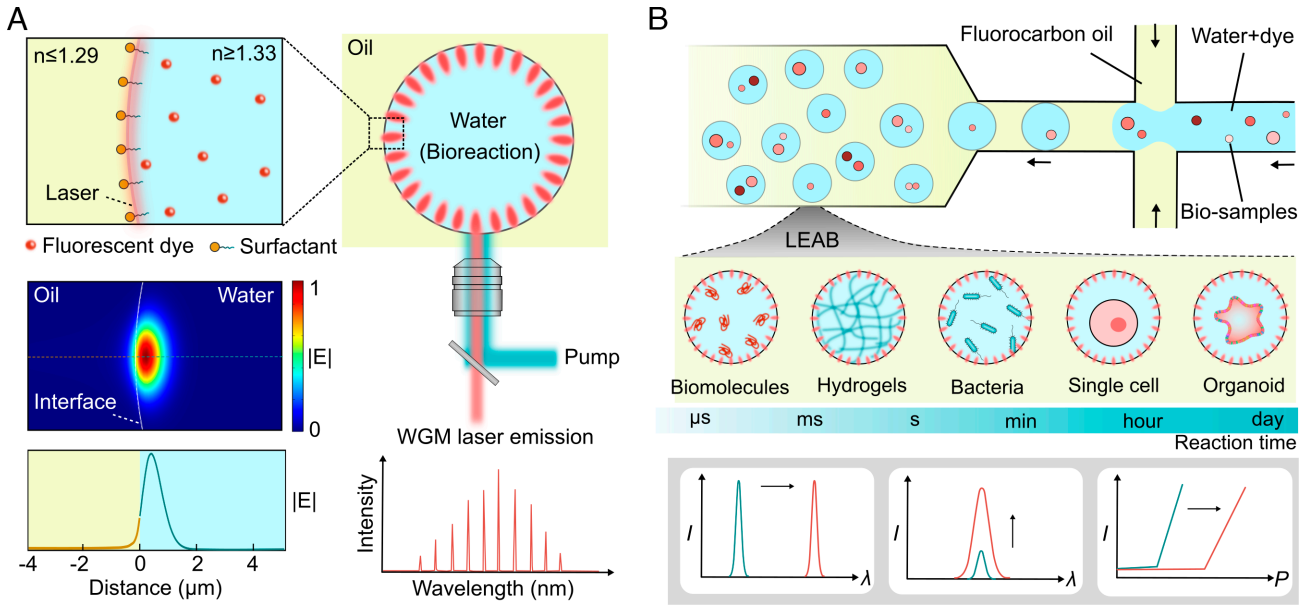

Fig. 1. Concept of laser-emitting aqueous bioreactors (LEABs) in fluorocarbon oils. (*A*) Water-in-oil LEABs. The water droplets, doped with organic dye as the gain medium, reside in fluorocarbon oil with surfactant for stability. The fluorocarbon oil has an RI of ≤1.29, whereas the aqueous droplets containing bioactive materials have an RI ≥ 1.33. Laser signals, modulated by internal reactions, provide real-time insights into reaction processes. In addition, the reactions inside the droplets can interact with the primary resonating energy, promising an enhanced sensitivity. (*B*) LEABs can encapsulate various bioactive materials, functioning as bioreactors. The microfluidic droplet technique facilitates the large-scale production of LEABs for high-throughput analysis. By preventing evaporation, this setup enables monitoring of reactions over durations ranging from microseconds to several days, leveraging the unique behaviors of laser emission.

(Fig. 1*B*). This enables real-time and long-term monitoring of bioreactions through distinct laser signals, such as spectral wavelength shifts and lasing threshold behaviors. Additionally, the strong interaction between bioreactions and the primary resonating energy enhances sensitivity by two orders of magnitude compared to conventional WGM lasers. By leveraging microfluidic droplet technology, LEABs can be mass-produced with uniform lasing characteristics, facilitating high-throughput analysis at the picoliter scale. We demonstrated their utility in enzyme evaluation and metabolic analysis at single-cell and multicellular levels, as well as laser threshold-gated screening for single yeast cells. This study can potentially bridge the critical gap between laser technology and biochemical applications, significantly expanding the scope of laser-assisted biochemical discoveries.

Results

Optical Characterization of Water-In-Oil LEABs. Water-in-oil LEABs can be generated via simple vortex emulsification or microfluidic droplet techniques, enabling precise control over droplet size (*SI Appendix*, Fig. S1 *A–C*). As a proof of concept, fluorescein isothiocyanate (FITC) solution at a concentration of 3 mM was introduced as the gain medium. FC-84 (RI ~1.26) was used as the oil phase with 2% surfactant to stabilize the droplets. Droplet sizes can range from several micrometers to hundreds of micrometers, with this study focusing on droplets around 100 μm in diameter.

When a droplet was illuminated by a pulsed laser at 480 nm (*SI Appendix*, Fig. S2), laser emission was generated due to the resonating of WGMs (Fig. 2 *A* and *B* and Movie S1). When the central area was pumped, a bright lasing ring appeared at the circumference of the droplets (Fig. 2 *B*, *Inset* and *SI Appendix*, Fig. S3*A*). Droplets generated via microfluidics exhibited uniform size, ensuring consistent laser emission from each droplet (Movie S2). When the edge was pumped, two bright lasing points were observed at the circumference (*SI Appendix*, Fig. S3*B*).

As the pump intensity increased, a distinct lasing threshold was observed (Fig. 2*C*). Typically, 100 μm LEABs containing deionized water exhibited a uniform threshold of ~16.7 ± 1.3 μJ mm^{-2} (Fig. 2*D* and *SI Appendix*, Fig. S4 and Movie S3). The spectrum showed comb-like lasing peaks when the pump intensity exceeded the threshold. The full width half maximum (FWHM) of the lasing peaks was ~ 0.07 nm, corresponding to a Q-factor of 7986, calculated using the equation $Q = \lambda_R/\lambda_{FWHM}$, where λ_R is the wavelength of the resonating peak and λ_{FWHM} is the FWHM. Even at larger diameters, such as ~200 μm, lasing emission was still generated, with denser laser peaks (*SI Appendix*, Fig. S5 *A* and *B*). The minimum diameter of pure water LEABs that could support laser emission was ~65 μm (*SI Appendix*, Fig. S5*C*). The lasers remained stable within 15,000 pump pulses under 5× threshold intensity (*SI Appendix*, Fig. S5*D*).

The minimum lasing size of LEABs is significantly influenced by their RI. Typically, the RI of biological aqueous solutions ranges from 1.33 to 1.40 (33, 34). We investigated the minimum lasing diameter of the LEABs in fluorocarbon oil (FC-84) as a function of varying RIs (Fig. 2*E*). To adjust the RI of the LEABs, we utilized common aqueous solutions, including cell culture medium, Poly(ethylene glycol) (PEG) solutions, and glycerol. LEABs with RIs between 1.33 and 1.34 (e.g., DMEM with 10 vol% fetal bovine serum) exhibited a minimum lasing diameter of 50 to 65 μm (*SI Appendix*, Fig. S5*E*). As the RI increased, the minimum lasing diameter gradually decreased. For instance, LEABs containing 50 vol% glycerol (RI ~1.405) showed a minimum lasing diameter of 18 μm, with fewer lasing peaks and a free spectral range of ~2.88 nm (*SI Appendix*, Fig. S5*F*).

LEABs containing other organic dyes, such as Rhodamine B, exhibited similar lasing performance under appropriate pump intensity, with corresponding laser peaks occurring between 600 and 650 nm (*SI Appendix*, Fig. S6). LEABs maintained stable lasing performance even when the RI of the fluorocarbon oil increased to 1.29 (e.g., FC-40) (*SI Appendix*, Fig. S7 *A* and *B*). Notably, conventional aqueous WGM droplet lasers typically

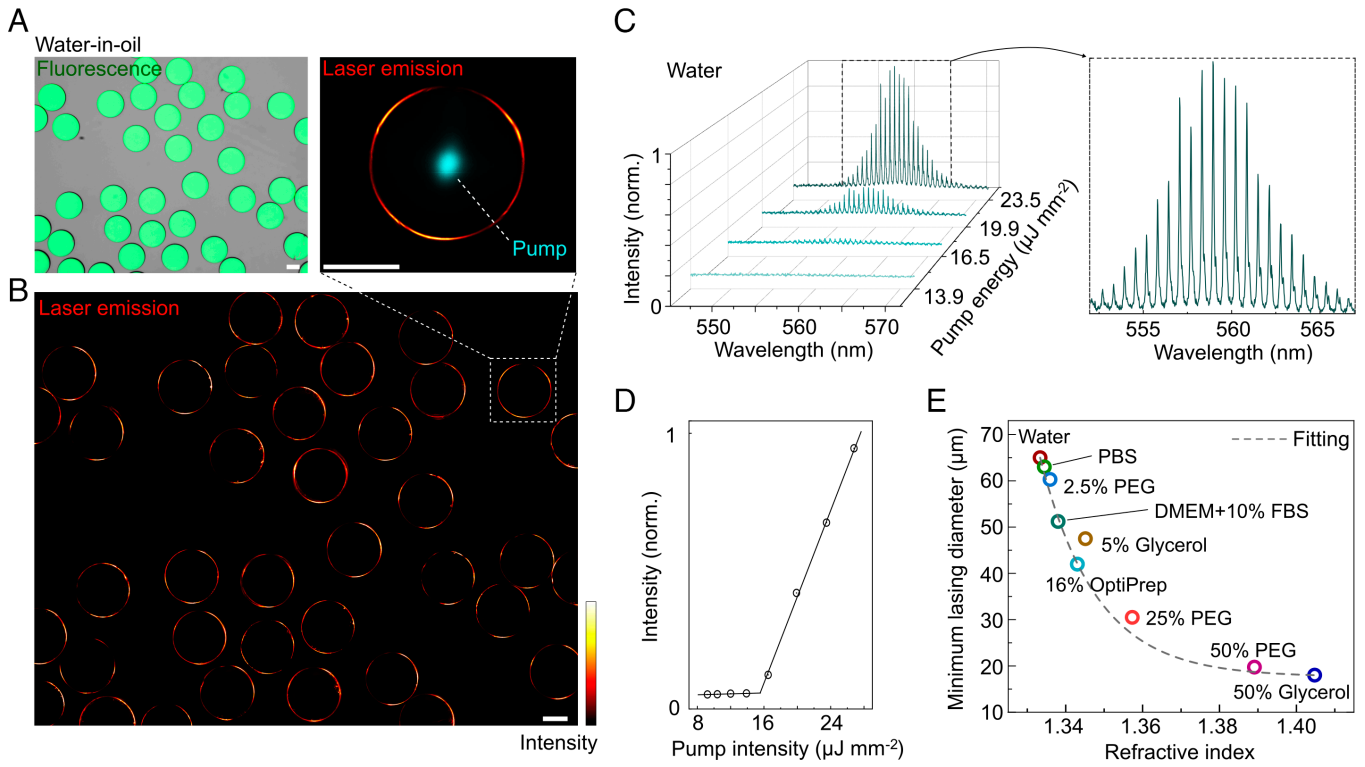

Fig. 2. Characterization of the LEABs in fluorocarbon oil (FC-84). (*A*) Fluorescence image of the LEABs with uniform size generated by microfluidic droplet technique. (*B*) Laser emission image of the droplets. Each droplet can generate the laser emission under the same pump intensity owing to its uniform size. The pump light was removed in this image. The inset is a laser emission image with the pump light. The red color of the laser emission is the false color for visualization. (Scale bar, 50 μm.) (*C*) Laser spectra when the pump intensity increased. (*D*) Spectral integrated intensities as a function of pump intensity. A clear threshold behavior was observed. (*E*) Minimum lasing diameter of the LEABs when the refractive index (RI) of the aqueous phase increased.

survive for less than 100 s in air due to rapid evaporation. Although adding glycerol can extend their lifetime to a few minutes, long-term monitoring remains challenging. However, their lifespan is extended to several days by encasing droplets in fluorocarbon oil, representing a more than 1,000-fold increase (*SI Appendix*, Fig. S7*C*).

Lasing Performance in Double-Emulsion LEABs. The water–oil emulsion also forms double-emulsion droplets, such as the water-in-oil-in-water (W/O/W) and oil-in-water-in-oil (O/W/O) configurations. We investigated the lasing performance of LEABs under these conditions. W/O/W droplets were fabricated with the inner aqueous phase containing FITC (Fig. 3*A*). The thickness of the oil shell was ~13 μm. When illuminated, a bright lasing ring appeared along the circumference of the inner aqueous core. Additionally, W/O/W droplets containing two or three aqueous cores were produced, with each core supporting lasing emission when the entire droplet was pumped. However, lasing only occurred in the noncontacting regions due to the disruption of light resonance at the interface contacts. Similarly, O/W/O droplets with a FITC aqueous shell also supported laser emission (Fig. 3*B* and *SI Appendix*, Fig. S8). However, in this case, only two lasing spots were observed at the circumference.

We compared the laser thresholds for three configurations: water-in-oil, W/O/W, and O/W/O (Fig. 3*C*). For similarly sized aqueous cores, water-in-oil droplets exhibited the lowest threshold (~16.7 μJ mm^{-2}), whereas W/O/W droplets had a threshold approximately 3.6 times higher (~60.3 μJ mm^{-2}). O/W/O droplets showed an intermediate threshold of ~33.6 μJ mm^{-2}. The shell thickness significantly influenced lasing behavior. The shell refers to the oil layer in W/O/W droplets and the water layer in O/W/O droplets. With increasing RI of the aqueous part, the minimum shell thickness enabling laser emission decreased (Fig. 3*D*). For example, with pure water as the aqueous part, the minimum shell thickness was ~12 μm. When the RI increased to ~1.4, the minimum oil shell thickness in W/O/W droplets was ~6.1 μm, whereas the minimum aqueous shell thickness in O/W/O droplets reduced to ~2.5 μm. This relationship was tested with an inner core diameter of ~100 μm. Furthermore, increasing the RI of the aqueous core allowed for a smaller overall droplet size. For instance, the O/W/O droplet diameter (including the aqueous shell) could be reduced to ~30 μm when the RI of the aqueous part reached ~1.4 (Fig. 3*E*).

When pure water is used as the aqueous phase, the minimum shell thickness observed (~12 μm) is much larger than the typical range of the evanescent field (a few micrometers). We believe that this is due to the following reasons. In O/W/O droplets, thinner shells contain less fluorescent dye, leading to an increased lasing threshold. Similarly, in W/O/W droplets, thinner shells also raise the lasing threshold, likely due to energy loss from light absorption by the outer aqueous phase, which contains the surfactant SDS (sodium dodecyl sulfate). SDS can absorb light (35), contributing to this threshold increase. All our measurements were done using pump energies below ~352.7 μJ mm^{-2}, as higher energy can cause the double-emulsion droplets unstable or even collapse. Consequently, under this energy constraint, the observed minimum shell thickness tends to be larger.

LEABs for Ultrasensitive Sensing of Bioreactions. The water–oil emulsion also forms double-emulsion droplets. LEABs facilitate bioactivity analysis through their unique laser spectrum. The sensing mechanism of WGM sensors typically employs the resonant wavelength interrogation technique (36). Conventional WGM sensors utilize the beads (such as polystyrene beads, glass beads, etc.)

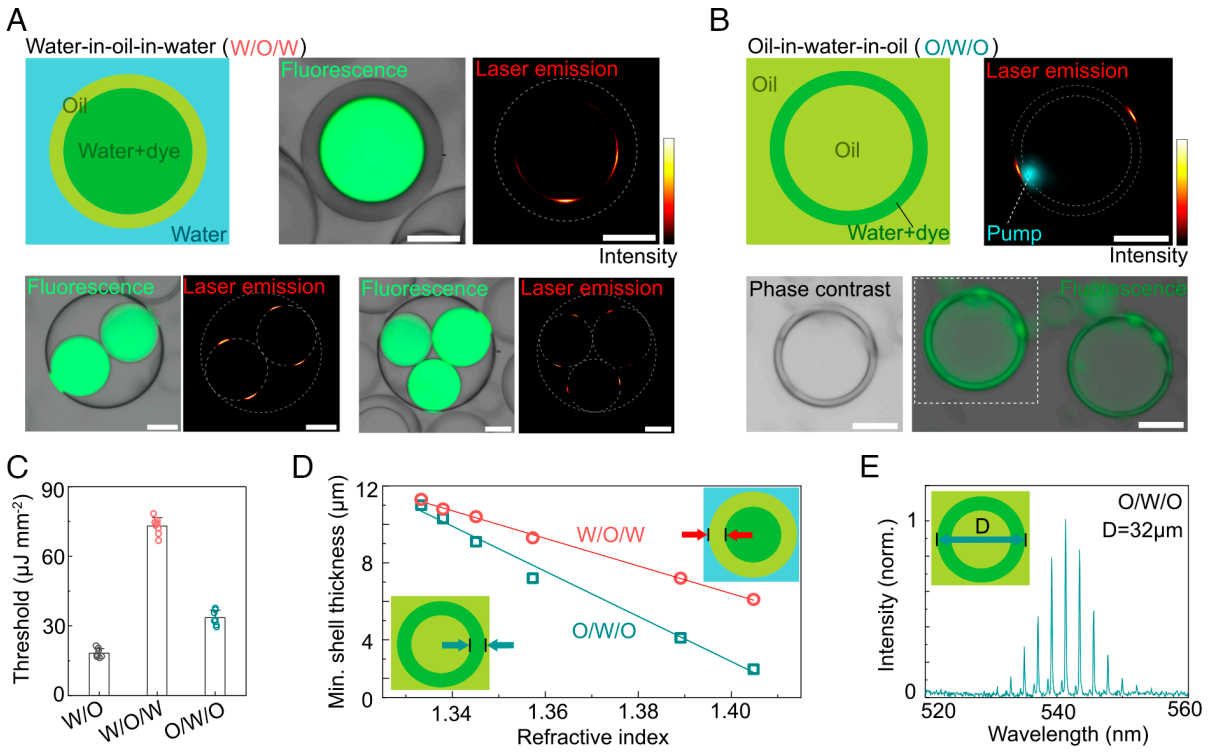

Fig. 3. Characterization of laser behaviors in double-emulsion LEABs. (*A*) Laser emission in W/O/W droplets. Laser emission was observed in droplets with single, double, and triple aqueous cores. The pump light was removed in this image. (Scale bar, 50 μm.) (*B*) Laser emission in O/W/O droplets. Droplets with a single aqueous shell exhibited laser emission. (*C*) Laser threshold comparison among the single-emulsion (W/O) droplets, W/O/W droplets, and O/W/O droplets. (mean ± SD, statistic number N = 8, 8, 7) (*D*) Minimum shell thickness required for laser emission as the RI of the aqueous phase increased. Insets illustrate the shell thickness. The investigation was conducted under pump energies below ~352.7 μJ mm^{-2}. (*E*) Laser spectrum of an O/W/O droplet with a 32 μm diameter and a 1.4 RI in aqueous shell. The inset illustrates the diameter of the O/W/O droplet.

or glass capillary as the resonators, which are filled with biological solutions around the beads or within the capillary (19, 37, 38) (Fig. 4 *A*, *I* and *II*). Biological activities or reactions in these aqueous solutions cause perturbations in the net optical path length or the electromagnetic boundary conditions, resulting in a shift in the resonant spectrum. This shift can be described by the equation (39):

$$\frac{\Delta\lambda}{\lambda} = \frac{\Delta n_{eff}}{n_{eff}} + \frac{\Delta R}{R}, \quad [1]$$

where λ is the resonate wavelength, and R is the radius of the resonator. Part of the mode extends outside the resonator as an evanescent field, leading to the effective RI given by (39):

$$n_{eff} = \frac{\int n(r)E(r)^2 dr}{\int E(r)^2 dr}, \quad [2]$$

where n is the RI along the radius, and E is the electric field. Changes in the RI due to biological activities in the solution will alter n_{eff}, enabling the analysis of bioactivities within the droplets.

Using the 100 μm diameter resonator as an example, we employed finite element analysis to investigate the electric field distribution in polystyrene (PS) WGM lasers, glass capillary WGM lasers, and LEABs (Fig. 4*A* and *SI Appendix*, Fig. S9*A*). For the glass capillary, the thickness was set to 1 μm. The results revealed that the laser mode volume was almost entirely confined within the WGM resonators. In conventional WGM lasers (Fig. 4 *A*, *I* and *II*), bioreactions occurring in water interact only with the evanescent component of the mode (38, 40). Conversely, in water-in-oil LEABs, the mode volume almost completely overlaps with the biological phase (Fig. 4 *A*, *III*). According to Eq. **2**, this configuration can significantly enhance the effective RI change (*SI Appendix*, Fig. S9*B*), theoretically resulting in a larger wavelength shift.

For 100 μm diameter resonators, the sensitivity to RI changes was 373.0 nm RIU^{-1} for the water-in-oil LEABs, compared to 1.9 nm RIU^{-1} for the PS bead laser and 3.1 nm RIU^{-1} for the glass capillary laser (Fig. 4*B*). This represented a sensitivity enhancement of 196-fold and 120-fold, respectively. Typically, smaller PS beads or glass capillaries can release a stronger evanescent field in aqueous environments, thereby enhancing sensitivity. For instance, 10 μm PS microlasers can achieve a sensitivity of ~ 23.3 nm RIU^{-1} (18). This demonstrates that the proposed LEABs still exhibit more than an order of magnitude improvement in sensitivity compared to smaller conventional microlasers. With a spectral resolution of approximately 1 pm, the RI resolution achieved by LEABs can be 2.7×10^{-6}. It is important to note that the 1 pm resolution is obtained after performing Gaussian peak fitting on the initial resolution of 40 pm from the spectrometer (18). This substantial enhancement was also observed in resonators with other sizes (*SI Appendix*, Fig. S9 *C* and *D*). Consequently, LEABs present as effective bioreactors for ultrasensitive analysis compared to conventional WGM sensors.

As a proof of concept, we utilized this tool to evaluate enzyme activities in a label-free manner (Fig. 4*C*). Trypsin and Bovine serum albumin (BSA) were encapsulated inside the droplets to monitor BSA hydrolysis by trypsin, with FITC added as the gain medium. The hydrolysis of BSA into smaller fragments increased the RI of the aqueous solutions, shifting the laser spectrum wavelength (Fig. 4*C*). Due to the higher density of fluorocarbon oils compared to water, we designed an inverted microwell array to localize the LEABs and ensure their complete immersion in oil

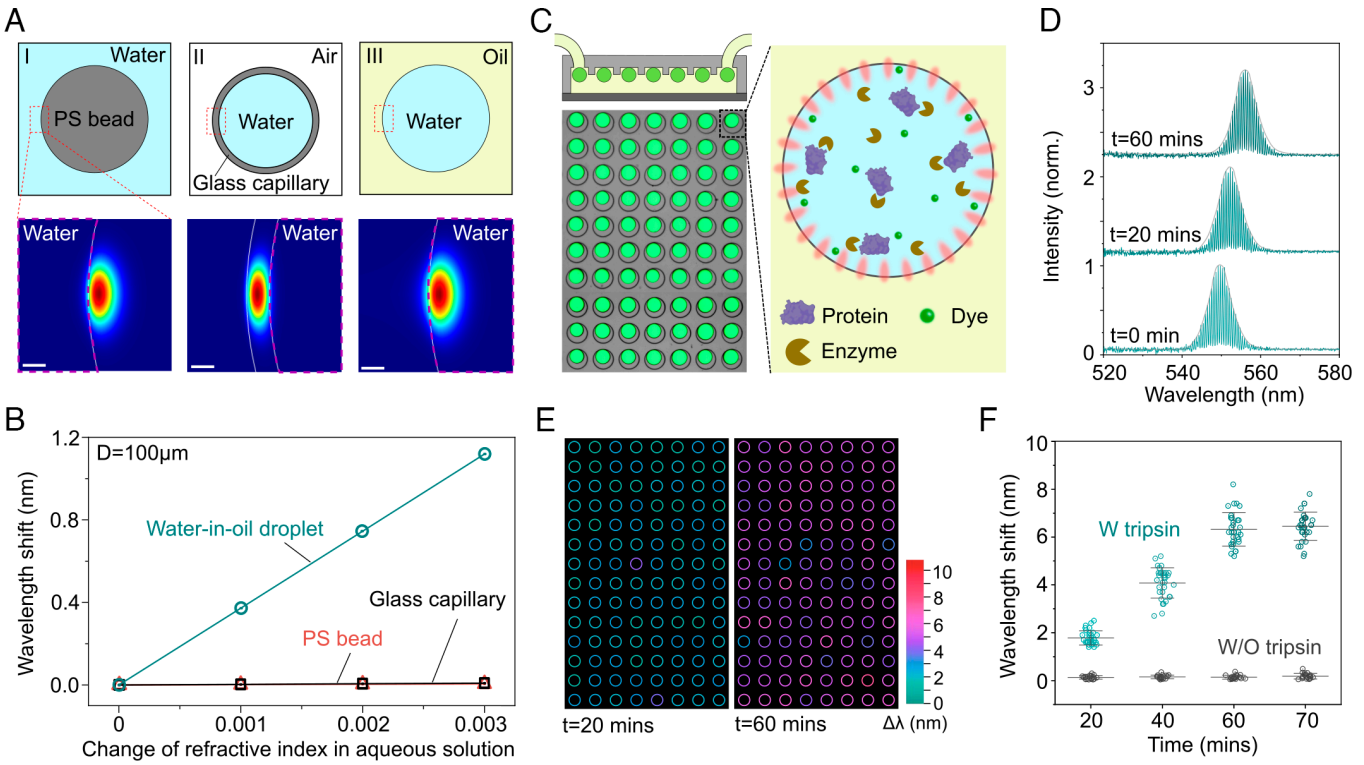

Fig. 4. LEABs for ultrasensitive enzyme evaluation. (*A*) Configurations of WGM lasers as biosensors and their distribution of basic-mode electrical field: PS bead laser (I), glass capillary laser (II), and the water-in-oil LEAB (III). The thickness of the glass capillary was set as 1 μm. The reaction in the LEABs can interact with most of the resonant energy, effectively inducing changes in the laser spectrum. (Scale bar, 1 μm.) (*B*) Theoretical analysis of wavelength shift versus RI change in aqueous solutions. The resonator diameter was set to 100 μm. (*C*) Microwell array for high-throughput evaluation of enzyme effects on proteins. Green spheres are the fluorescence images of the LEABs captured in the microwells. (*D*) Wavelength shift during the reaction of trypsin and BSA. (*E*) Visualization of wavelength shift of the droplet lasers in the microwell array. (*F*) Statistical analysis of the wavelength shift during the enzyme reaction over 70 mins. The shift started to saturate at ~70 mins (mean ± SD).

(Fig. 4*C* and *SI Appendix*, Fig. S10 *A*–*D*). This configuration enables high-throughput analysis and accommodates variations across biological samples effectively. After approximately an hour of reaction, we observed a significant red shift (~6 nm) in the laser spectrum (Fig. 4*D*). Variations in reaction rates were also observed among droplets (Fig. 4*E*). Statistical analysis indicated that the wavelength shift saturated after ~70 mins, with an average shift of ~6.4 nm. In WGM lasers, wavelength shifts are influenced by changes in RI, variations in dye concentration (e.g., due to photobleaching), and droplet size (41). In our experiments, droplet size remained constant, and its impact on the spectral shift was negligible. To eliminate the influence of dye concentration, we conducted control experiments. Droplets lacking either trypsin or BSA showed no significant spectral shift (Fig. 4*F* and *SI Appendix*, Fig. S10*E*), confirming that the observed shift was not caused by photobleaching. High-temporal-resolution spectra confirmed a continuous red shift in the laser peaks (*SI Appendix*, Fig. S10*F*). Following the above result, the BSA hydrolysis by trypsin induced an RI change of 0.017, aligning well with measurements obtained using a commercial refractometer (ORF 1RS, KERN OPTICS) (*SI Appendix*, Fig. S10*G*).

LEABs for High-Throughput Cellular Metabolism Analysis. LEABs have significant potential in high-throughput cell analysis at single-cell and multicellular levels. Here, we employed the LEABs for cellular metabolism analysis as a proof of concept. Typically, tumor cells exhibit rapid glucose consumption, with most of the glucose-derived carbon being secreted as lactate, a phenomenon known as the Warburg effect (42) (Fig. 5*A*). This can lead to a decrease in pH within the droplet when a cell is encapsulated inside. Therefore, the pH in the droplet can reflect the metabolism state of the cell. We adjusted the cell concentration to ensure that most droplets contained a single cell, facilitating single-cell level analysis (Fig. 5*B*).

We introduced the FITC as the gain medium of LEABs, with each droplet containing ~ 0.5 nL of solution. The lasing threshold of LEABs containing single cells showed no significant difference compared to that of empty LEABs when the cells were initially encapsulated (*SI Appendix*, Fig. S11*A*). FITC, being a pH-sensitive dye, exhibits reduced fluorescence intensity at lower pH and increased intensity at higher pH (43) (Fig. 5*C*), which can also influence the laser signals. We examined the laser emission across a pH range of 3 to 9 under a fixed pump intensity set close to the lasing threshold of pH 3 droplets. Under these conditions, the laser emission intensity gradually increased with rising pH (Fig. 5*D* and *SI Appendix*, Fig. S11*B*). From pH 5 to pH 7, the laser intensity increased by 2.39-fold, whereas fluorescence intensity only increased by 0.08-fold. The difference in laser intensity was ~ 30 times greater than that in fluorescence intensity, attributable to the strong light–matter interactions within the laser cavity that amplify subtle changes.

Leveraging this feature, we investigated the single-cell metabolism of normal human dermal fibroblasts (NHDF) and lung tumor A549 cells. After 4 h incubation, we measured the laser intensity of LEABs containing single cells under the same pump intensity. The NHDF cells, with an average diameter of 13 to 15 μm, had a laser intensity centered around 0.58. Conversely, A549 cells, with a larger average diameter of 17 to 19 μm, exhibited a laser intensity centered around 0.43 (Fig. 5*E*). Based on the correlation between pH and laser intensity, the average pH in NHDF

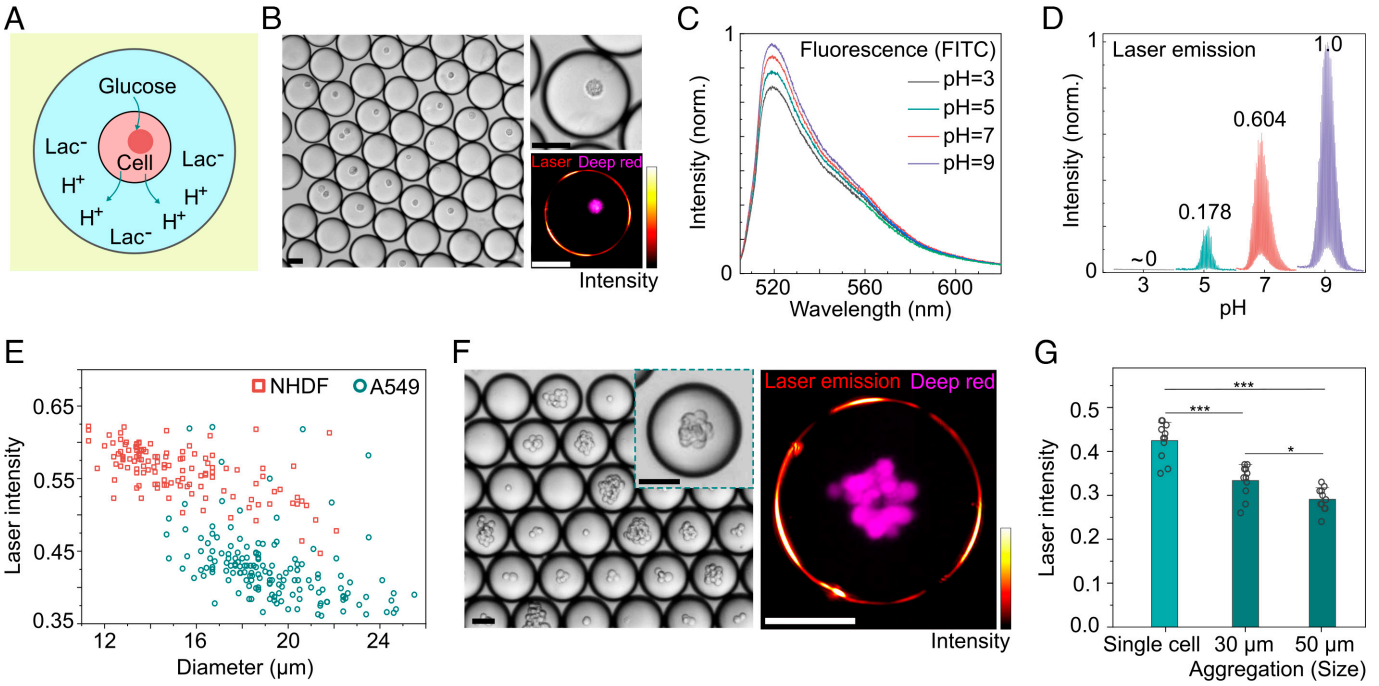

Fig. 5. Cell metabolism analysis via LEABs. (*A*) Schematic of pH change in LEABs induced by cell consumption of glucose and generation of lactate. (*B*) Single-cell encapsulation in LEABs. The inset is the merged laser emission image with the fluorescence image of the single cell. The cell was stained with cell tracker deep red. (Scale bar, 50 μm.) (*C*) FITC fluorescence in droplets at pH of 3, 5,7, and 9. (*D*) Laser emission spectrum at pH of 3, 5,7, and 9. The pump intensity was adjusted close to the threshold of pH 3 droplet. (*E*) Laser intensity versus diameter of the NHDF and A549 cells (N = 125 for NHDF and 158 for A549). (*F*) Bright-field image and laser image of droplets containing multicellular A549 aggregates. (Scale bar, 50 μm.) (*G*) Comparison of laser intensity of droplets containing single cell, 30 μm multicellular aggregates, and 50 μm multicellular aggregates (mean ± SD, N = 11, 11, 11, **P* < 0.1, ****P* < 0.001).

droplets and A549 droplets was determined to be 6.7 and 6.1, respectively. Additionally, we observed a size-dependent correlation of laser intensity, particularly in A549 cells. Some droplets containing larger cells (~24 μm) had a laser intensity of ~ 0.37, corresponding to a pH of 5.9; this revealed significant metabolic heterogeneity.

We further explored the laser emission of LEABs containing multicellular aggregates, focusing on their potential applications in in vitro models like spheroids and organoids. Multiple A549 cells were encapsulated in LEABs. After ~4 h of incubation, the cells formed multicellular aggregates (spheroids) within the droplets. By applying the appropriate pump intensity, laser emission was successfully achieved (Fig. 5*F*). The laser intensity results indicated a lower pH in droplets containing multicellular aggregates, exhibiting size-dependent behavior (Fig. 5*G*). For instance, LEABs with 30 μm aggregates showed an average intensity of 0.33, whereas those with 50 μm aggregates exhibited an average intensity of 0.29; this revealed the strong metabolic activity within the multicellular aggregates.

LEABs for Cellulase Analysis at the Single Yeast Level. We further showcased the laser threshold-gated cell screening based on LEABs. As a proof of concept, we assessed β-Glucosidase (BGL) secretion by a single yeast (S. cerevisiae) (44). We encapsulated individual yeast in reactors with saccharose and Fluorescein Di-β-D-Glucopyranoside (FDGlu). FDGlu, a nonfluorescent substrate for glucosidases, can be hydrolyzed into fluorescent fluorescein, which becomes the gain medium (Fig. 6 *A* and *B* and *SI Appendix*, Fig. S12). Protected by fluorocarbon oil, the droplets underwent long-term incubation. Over time, the droplets gradually exhibited fluorescence with varying intensities (*SI Appendix*, Fig. S13*A*). At 24 h, some droplets displayed highly bright fluorescence (Fig. 6*C*). The fluorescence intensity exhibited significant variation due to the heterogeneity among the yeast cells.

We tested the laser emission from the droplets and successfully achieved laser emission under proper pump intensity (Fig. 6 *D*–*E*). The different concentrations of fluorescein induced by heterogeneous enzyme activity resulted in various laser thresholds for the droplets. Some droplets with weak fluorescence could not generate laser emission (*SI Appendix*, Fig. S13*B*). Consequently, the droplets exhibited varying laser thresholds due to yeast heterogeneity. For instance, droplets I, II, and III in Fig. 6*C* exhibited thresholds of 35.5, 47.6, and 78.8 μJ mm^{-2}, respectively (Fig. 6*F*), even though the fluorescence in droplets I and II showed no obvious difference (*SI Appendix*, Fig. S13*C*). The statistical analysis of the LEABs (*SI Appendix*, Fig. S4) reveals that the slight size variations among the droplets have a negligible impact on the threshold. Consequently, the substantial fluctuations in threshold energy are primarily attributed to variations in fluorescein concentration.

We demonstrated threshold-gated screening of single yeast cells by adjusting the pump intensity. For instance, at a pump intensity of 55.6 μJ mm^{-2}, droplets I and II generated laser emission, whereas droplet III did not. When the pump intensity was reduced to 45.1 μJ mm^{-2}, only droplet I produced laser emission (Fig. 6*G*). This approach enabled the small fluorescence difference between droplets I and II (4.5% difference, *SI Appendix*, Fig. S13*C*) to be translated into an off-on distinction, enabling high-precision screening. As a control experiment, we designed droplets containing various FITC concentrations. The results demonstrated that with small differences in fluorescence, lasing threshold-gated screening could distinguish droplets with significantly higher precision (*SI Appendix*, Fig. S13 *D*–*E*).

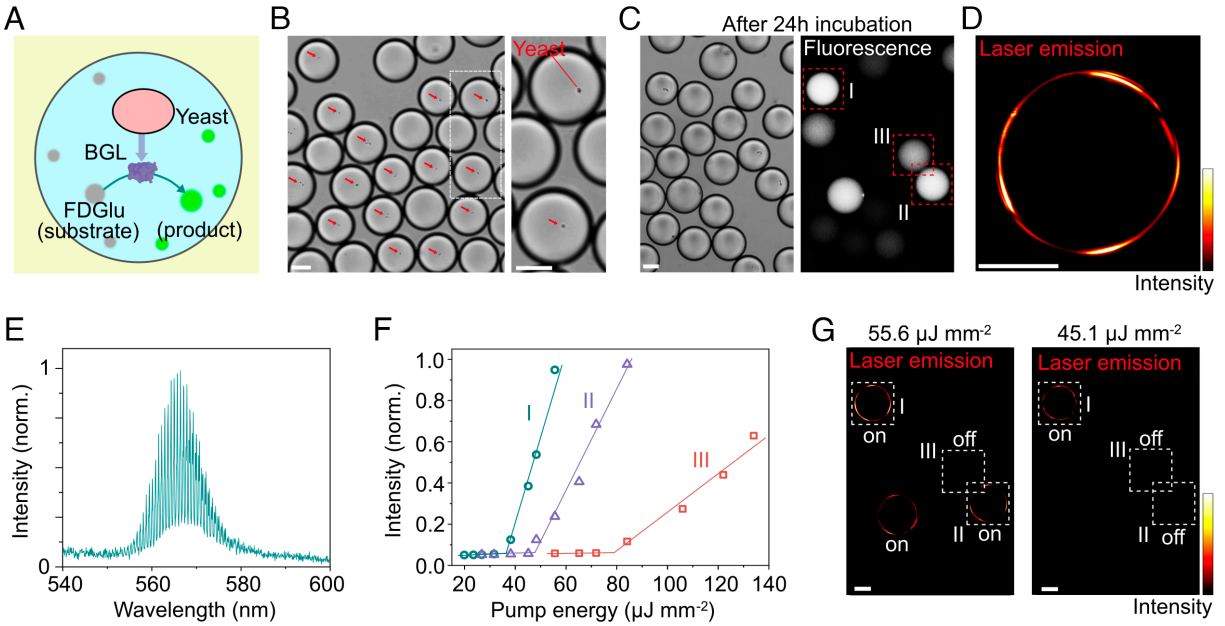

Fig. 6. LEABs for laser threshold-gated screening of cellulase secretion of single yeast. (*A*) Schematic of the reaction of nonfluorescent FDGlu to fluorescent product induced by the yeast-secreted BGL. (*B*) Encapsulation of a single yeast into the droplet for high-throughput analysis. The red arrow indicates the yeast. (*C*) Bright-field image and fluorescence image of the droplets after 24 h incubation. The droplets exhibited various fluorescent intensities due to the significant heterogeneity among yeasts. (*D*) Laser emission image of the droplet with yeast-induced fluorescein as the gain medium. The pump light was removed in this image. (*E*) A typical laser spectrum after 24 h incubation. (*F*) The emission intensity of droplets I, II, and III when increasing the pump intensity. It indicated droplets I, II, and III exhibited various laser thresholds. (*G*) Laser emission images of the droplets in Fig. 6*C* under the pump intensity of 55.6 and 45.1 μJ mm^{-2}, respectively. The pump light was removed in this image. (Scale bar, 50 μm.)

Discussion

Laser emission holds significant potential in biological and biochemical applications. In this study, we proposed microfluidic LEABs in fluid environments, offering several key advantages. First, LEABs function as laser emitters and biological microreactors, enabling long-term incubation and analysis with stable laser output, thereby overcoming the rapid evaporation issue faced by aqueous droplet lasers in the air. Second, bioreactions within LEABs directly interact with the majority of resonating light, resulting in ultrasensitive laser signal responses to changes inside the droplets; this contrasts with conventional WGM sensors, where the sensing relies on the evanescent field, a small fraction of the resonating light. Third, compared to fluorescence signals, laser emission offers multiple unique features, including spectral shift, nonlinear lasing threshold, and lasing images. Fourth, by integrating microfluidic techniques, LEABs enable high-throughput analysis at single-cell and multicellular levels.

The integration of microlasers with microfluidic droplet reactors opens up a wide range of applications. For instance, LEABs could enable the development of laser-emitting flow cytometry with improved precision, providing imaging and spectral information in a high-throughput format using high-speed spectrometers and cameras. This advancement could extend laser technology to areas such as digital analysis and PCR. Furthermore, LEABs could analyze the water-solvent catalytic reactions, offering an ultrasensitive tool for real-time monitoring via laser signals.

Materials and Methods

Water-In-Oil Droplet Generation. The water-in-oil droplets were fabricated with the direct vortex method and microfluidic droplet technique. The oil phase was tested by fluorocarbon oil including FC-84 (RI ~1.25), FC-40 (RI ~1.29), and HFE-7500 (RI ~1.29) (3 M, China suppliers). To stabilize the droplets, 2 wt% surfactant (008-FluoroSurfactant, RAN Biotechnologies) was added into the oil phase.

For the vortex method, 100 μL aqueous solution with ~3 mM FITC (fluorescein sodium salt, Sigma) was added into the 1 mL oil phase in a 2 mL tube. Then, the solution was vortexed for ~20 s to achieve the water-in-oil droplets. For the microfluidic droplet technique, the aqueous phase and oil phase were introduced into a flow-focusing droplet chip. By adjusting the size of the junction and the flow speed, the droplets size can be adjusted. The generated droplets were collected into the oil phase in the microtube.

W/O/W Double-Emulsion Droplets Generation. First, water-in-oil single-emulsion droplets were generated with uniform size via the microfluidic droplet technique. Then, 100 μL droplet solution was added into 1.5 mL water, which followed the vortex to form the W/O/W double-emulsion droplets. 2 wt% Tween 20 was added into the outside water solution to stabilize the system.

O/W/O Double-Emulsion Droplets Generation. Similarly, the oil-in-water single-emulsion droplets were generated with uniform size via the microfluidic droplet technique. Then, 100 μL droplet solution was added into 1.5 mL oil solution, which followed the vortex to form the W/O/W double-emulsion droplets. Both inner and outer oil phases were added 2 wt% surfactant.

Laser Characterization. All components were integrated into a Nikon Ni-E upright confocal microscope. A 10X objective was used for excitation and signal collection. The pulsed laser (EKSPLA NT230, 50 Hz, 5 ns pulse width) with a parameter oscillator (OPO) was used as an optical pump. The excitation was set at 480 nm for FITC and 550 nm for Rhodamine B. The laser emission was split by a beam splitter and sent to a spectrometer with 40 pm spectral resolution (Andor Kymera 328i with 1800 lines per mm grating and Newton 970) and a camera (Photron, FASTCAM Mini UX 50) for spectrum and image.

Microfluidic Chip Fabrication. The fabrication of the microfluidic droplet chip and the microwell chip followed a conventional lithography process, as outlined in our previous works. The microstructures were projected on SU-8 layer by a UV lithographer (UV Litho-ACA, TuoTuo Technology Pte. Ltd.). When the SU-8 mold was ready, Polydimethylsiloxane (PDMS) was used to fabricate the microfluidic chip, followed by the bonding with glass slides to form the sealed microfluidic channels.

Cell Culture. The A549 and NHDF cells from ATCC were cultured in DMEM supplemented with 10% fetal bovine serum (FBS) and 100 U mL^{-1} penicillin/streptomycin. Cells were incubated in a standard incubator with 5% CO_2 at 37 °C. The cells were used after 3 to 4 passages.

Single-Cell Encapsulation and Multicellular Aggregate Formation. For single-cell encapsulation, the final cell concentration was adjusted to 2×10^6. For the multicellular aggregate formation, the final A549 concentration was adjusted to 2×10^7. After the encapsulation, the droplets were immediately transferred into an incubator. After 4 h incubation, the cells formed the aggregates inside the droplets.

Cell Metabolism Experiment. Before encapsulation, the cells were cultured in DMEM without D-glucose. For encapsulation, the cell suspension and a 20 mM glucose solution containing 3 mM FITC were simultaneously introduced into two inlets on the microfluidic chip at a 1:1 flow ratio. After emulsification, the droplet suspension was incubated for 4 h.

Yeast Culture, Encapsulation, and Laser Characterization. Yeasts from *S. cerevisiae* (YSC2, Sigma) were cultured in the 50 mg mL^{-1} saccharose solution at 30 °C. For single-yeast analysis, the yeast concentration was adjusted to 3×10^6 in the solution containing 50 mg mL^{-1} saccharose and 3 μM FDGlu. The droplets in the oil were introduced in a microfluidic chip for long-term incubation at 30 °C. After incubation, the droplets were pumped by 485 nm light to investigate the laser emission.

Statistical Analysis. The data were presented as mean ± SD. Two-tailed *t* test was used to reveal the statistical difference with Origin 8.0. A *P*-value less than 0.001 was considered as a significant difference (***$P < 0.001$).

Data, Materials, and Software Availability. All study data are included in the article and/or supporting information.

ACKNOWLEDGMENTS. This work was supported by the A*STAR MTC IRG-Grant (M21K2c0106, Singapore) and the NSW Government through the Cancer Institute NSW. We would like to thank the support from MOE Acrf Tier 1 grant under No. RG69/24.

Author affiliations: [a]School of Biomedical Engineering, University of Technology Sydney, Sydney, NSW 2007, Australia; [b]School of Electrical and Electronics Engineering, Nanyang Technological University, Singapore 639798, Singapore; [c]Department of Electrical and Systems Engineering, Washington University, St Louis, MO 63130; [d]Department of Bioengineering and Therapeutic Sciences, University of California San Francisco, San Francisco, CA 94158; and [e]Institute for Biomedical Materials and Devices, Faculty of Science, University of Technology Sydney, Sydney, NSW 2007, Australia

Author contributions: G.F., P.-H.T., D.J., and Y.-C.C. designed research; G.F., P.-H.T., T.Z., and H.Z. performed research; G.F., J.L., and S.Z. contributed new reagents/analytic tools; G.F., P.-H.T., J.L., T.Z., H.L., H.Z., D.J., and L.Y. analyzed data; and G.F. and Y.-C.C. wrote the paper.

1. L. Mazutis *et al.*, Single-cell analysis and sorting using droplet-based microfluidics. *Nat. Protoc.* **8**, 870–891 (2013).
2. M. T. Guo, A. Rotem, J. A. Heyman, D. A. Weitz, Droplet microfluidics for high-throughput biological assays. *Lab Chip* **12**, 2146–2155 (2012).
3. J.-C. Baret *et al.*, Fluorescence-activated droplet sorting (FADS): Efficient microfluidic cell sorting based on enzymatic activity. *Lab Chip* **9**, 1850 (2009).
4. M. M. Eric Brouzesa *et al.*, Droplet microfluidic technology for single-cell high-throughput screening. *Proc. Natl. Acad. Sci.* **106**, 14195–14200 (2009).
5. X. Fan, S. H. Yun, The potential of optofluidic biolasers. *Nat. Methods* **11**, 141–147 (2014).
6. Y. C. Chen, X. Fan, Biological lasers for biomedical applications. *Adv. Opt. Mater.* **7**, 1900377 (2019).
7. Z. Korenjak, M. Humar, Smectic and soap bubble optofluidic lasers. *Phys. Rev. X* **14**, 011002 (2024).
8. G. Pirnat, M. Marincic, M. Ravnik, M. Humar, Quantifying local stiffness and forces in soft biological tissues using droplet optical microcavities. *Proc. Natl. Acad. Sci. U.S.A.* **121**, e2314884121 (2024).
9. V. M. Titze *et al.*, Hyperspectral confocal imaging for high-throughput readout and analysis of bio-integrated microlasers. *Nat. Protoc.* **19**, 928–959 (2024).
10. J. L. Jiawei Wang *et al.*, Revealing molecular diffusion dynamics in polymer microspheres by optical resonances. *Sci. Adv.* **9**, eadf1725 (2023).
11. H. Yamagishi *et al.*, Pneumatically tunable droplet microlaser. *Laser Photon. Rev.* **17**, 2200874 (2023).
12. M. C. Gather, S. H. Yun, Single-cell biological lasers. *Nature* **5**, 406–410 (2011).
13. M. Humar, S. H. Yun, Intracellular microlasers. *Nat Photonics* **9**, 572–576 (2015).
14. A. H. Fikouras *et al.*, Non-obstructive intracellular nanolasers. *Nat. Commun.* **9**, 4817 (2018).
15. Y. C. Chen *et al.*, Laser-emission imaging of nuclear biomarkers for high-contrast cancer screening and immunodiagnosis. *Nat. Biomed. Eng.* **1**, 724–735 (2017).
16. G. Fang *et al.*, Single-cell laser emitting cytometry for label-free nucleolus fingerprinting. *Nat. Commun.* **15**, 7332 (2024).
17. G. Fang *et al.*, Compressible hollow microlasers in organoids for high-throughput and real-time mechanical screening. *ACS Nano*, (2024).
18. M. Schubert *et al.*, Monitoring contractility in cardiac tissue with cellular resolution using biointegrated microlasers. *Nature Photonics* **14**, 452–458 (2020).
19. N. Toropov *et al.*, Review of biosensing with whispering-gallery mode lasers. *Light Sci. Appl.* **10**, 42 (2021).
20. T. Zhou *et al.*, Digital lasing biochip for tumor-derived exosome analysis. *Anal. Chem.* **97**, 5605–5611 (2025).
21. H. Azzouz *et al.*, Levitated droplet dye laser. *Opt. Express* **14**, 4374–4379 (2006).
22. S. Maayani, L. L. Martin, T. Carmon, Water-walled microfluidics for high-optical finesse cavities. *Nat. Commun.* **7**, 10435 (2016).
23. J. T. Marmolejo, A. Canales, D. Hanstorp, R. Méndez-Fragoso, Fano combs in the directional Mie scattering of a water droplet. *Phys. Rev. Lett.* **130**, 043804 (2023).
24. T. W. Hänsch, Edible lasers and other delights of the 1970s. *Opt. Photonics News* **16**, 14–16 (2005).
25. D. McGloin, Droplet lasers: A review of current progress. *Rep. Prog. Phys.* **80**, 054402 (2017).
26. J. Schäfer *et al.*, Quantum dot microdrop laser. *Nano Lett.* **8**, 1709–1712 (2008).
27. A. Jonas *et al.*, In vitro and in vivo biolasing of fluorescent proteins suspended in liquid microdroplet cavities. *Lab Chip* **14**, 3093–3100 (2014).
28. S.-X. Qian, H.-M. Tzeng, R. K. Chang, Lasing droplets: Highlighting the liquid–air inte ace by laser emission. *Science* **231**, 486–488 (1986).
29. S. Avino *et al.*, Direct sensing in liquids using whispering-gallery-mode droplet resonators. *Adv. Opt. Mater.* **2**, 1155–1159 (2014).
30. S. Maayani, L. L. Martin, S. Kaminski, T. Carmon, Cavity optocapillaries. *Optica* **3**, 552 (2016).
31. G. A. Ferron, S. C. Soderholm, Estimation of the times for evaporation of pure water droplets and for stabilization of salt solution particles. *J. Aerosol Sci.* **21**, 415–429 (1990).
32. R. P. Melikhan Tanyeri, Ian M. Kennedy, Lasing droplets in a microfabricated channel. *Opt. Lett.* **32**, 2529–2531 (2007).
33. P. Y. Liu *et al.*, Cell refractive index for cell biology and disease diagnosis: Past, present and future. *Lab Chip* **16**, 634–644 (2016).
34. R. Barer, S. Tkaczyk, Refractive index of concentrated protein solutions. *Nature* **173**, 821–822 (1954).
35. I. A. Janković, M. Cakar, N. M. Jovan, Influence of sodium dodecyl sulfate on the reaction between Nile blue A and hydrogen peroxide. *J. Serb. Chem. Soc.* **64**, 359–364 (1999).
36. M. R. Foreman, J. D. Swaim, F. Vollmer, Whispering gallery mode sensors. *Adv. Opt. Photonics* **7**, 168–240 (2015).
37. F. Vollmer, L. Yang, Label-free detection with high-Q microcavities: A review of biosensing mechanisms for integrated devices. *Nanophotonics* **1** (3–4), 267–291 (2012).
38. A. François, N. Riesen, K. Gardner, T. M. Monro, A. Meldrum, Lasing of whispering gallery modes in optofluidic microcapillaries. *Opt. Express* **24**, 12466 (2016).
39. J. M. Ward, N. Dhasmana, S. Nic Chormaic, Hollow core, whispering gallery resonator sensors. *Eur. Phys. J. Spec. Top.* **223**, 1917–1935 (2014).
40. X. C. Yu *et al.*, Single-molecule optofluidic microsensor with interface whispering gallery modes. *Proc. Natl. Acad. Sci. U.S.A.* **119**, e2108678119 (2022).
41. M. Aas, A. Jonáš, A. Kiraz, Lasing in optically manipulated, dye-doped emulsion microdroplets. *Opt. Commun.* **290**, 183–187 (2013).
42. M. V. Liberti, J. W. Locasale, The warburg effect: How does it benefit cancer cells?. *Trends Biochem. Sci.* **41**, 211–218 (2016).
43. F. Guern, V. Mussard, A. Gaucher, M. Rottman, D. Prim, Fluorescein derivatives as fluorescent probes for pH monitoring along recent biological applications. *Int. J. Mol. Sci.* **21**, 9217 (2020).
44. P. Zhang, R. Zhang, S. Sirisena, R. Gan, Z. Fang, Beta-glucosidase activity of wine yeasts and its impacts on wine volatiles and phenolics: A mini-review. *Food Microbiol.* **100**, 103859 (2021).